frontiers | Frontiers in Energy Research

TYPE Original Research
PUBLISHED 27 February 2024
DOI 10.3389/fenrg.2024.1372060

OPEN ACCESS

EDITED BY
Chao Su,
China Jiliang University, China

REVIEWED BY
Tao Wang,
Southwest University, China
Bo Song,
Xi'an Jiaotong University, China
Jiang Pan,
China Jiliang University, China

*CORRESPONDENCE
Xinping Chen,
202321001@cqcet.edu.cn

RECEIVED 17 January 2024
ACCEPTED 16 February 2024
PUBLISHED 27 February 2024

CITATION
Chen X (2024), The adsorption and desorption processes of organic working fluids R1234yf, R134a, R32 in MOF-5 and Co-MOF-74: a molecular simulation study.
Front. Energy Res. 12:1372060.
doi: 10.3389/fenrg.2024.1372060

The adsorption and desorption processes of organic working fluids R1234yf, R134a, R32 in MOF-5 and Co-MOF-74: a molecular simulation study

Xinping Chen*

College of Artificial Intelligence and Big Data, Chongqing College of Electronic Engineering, Chongqing, China

The combination of nanoporous materials with organic working fluids holds the promise of further enhancing the performance of refrigerants based thermodynamics cycles. In this study, the adsorption and desorption properties of several organic refrigerants, e.g., R1234yf, R134a, R32, and their mixtures in metal-organic framework materials MOF-5 and Co-MOF-74 are investigated via molecular dynamics methods. The results indicate that the adsorption capacity is inversely proportional to the temperature during the adsorption process, and the adsorption capacity of the R1234yf/R32 mixture (molar ratio 2:1) is higher than that of the corresponding pure working fluids. The desorption amount, desorption regeneration rate, and desorption heat are directly proportional to the temperature. The interactions between different molecular atoms in the mixed working fluids promote the desorption process.

KEYWORDS

metal-organic frameworks, refrigerants, nanofluid, adsorption, molecular dynamics

1 Introduction

Energy serves as the foundation for the development of modern society. And its utilization reflects the level of scientific and economic strength of a country (Carbon, 2021). Therefore, the energy crisis and environmental pollution have drawn a lot of attentions. Thus, enhancing the efficiency of fossil fuel utilization and enlarging the scale of renewable energy are proposed to maintain the sustainable development of the world (Chen et al., 2019; Xiao et al., 2022).

So far, the thermodynamic cycles are the main approach for energy conversion. Organic Rankine Cycle (ORC) uses organic refrigerants as working fluids to recover the low-grade energies, e.g., industrial waste heat, geothermal energy and solar energy, which have a very good application prospects (Vivian et al., 2015; Zhang et al., 2019; Miao et al., 2020; Wang et al., 2024). However, the efficiency of ORC is relatively low because of the low temperature of heating source. Since the working fluid plays as the energy carrier in the thermodynamic cycles, the properties optimization of organic refrigerants could result in the efficiency enhancement of ORC (Su et al., 2017; Wang et al., 2020; Li et al., 2022). One practical method is using the zeotropic mixture as working fluids, which have extensively reported (Wang et al., 2019; McLinden and Huber, 2020; Zhu et al., 2021). Besides, McGrail et al. (2013) proposed to use metal-organic frameworks (MOFs) to enhance the properties of

refrigerants. This is the so called metal organic heat carriers (MOHCs). The adsorption energy is stored in MOFs at the condensation stage and then into thermal energy by desorbing the fluid molecules from MOFs during heating process.

MOFs are porous materials with periodic network structures formed by the self-assembly of metal ions or clusters and organic ligands through coordination (Kong et al., 2013). MOFs exhibit high specific surface area, large pore volume, and tunable structures, making them highly promising for applications in gas storage, heterogeneous catalysis, adsorption-based energy storage and other fields (Furukawa et al., 2013).

Qasem et al. (2018) investigated the adsorption of CO_2 by MOF-5 and MOF-177 under pressures ranging from 5 to 50 bar. The results showed that MOFs could store more CO_2 while consuming less energy compared to traditional storage systems. Wang et al. (2018) studied the adsorption and energy storage of R161 and similar refrigerants in MOF-5. It was found that fluorine atoms in the organic working pairs enhanced their adsorption in MOFs. Hu et al. (2018a), Hu et al. (2018b), Hu et al. (2019) investigated thermal energy storage properties of several refrigerants in MOF-74 and MOF-5. The results showed that the energy storage enhancement ratios of R1234yf, R1234ze and R134a with Mg-MOF-74 nanoparticles are higher than those of other M-MOF-74 (M = Co, Ni, Zn) materials.

In recent years, with the rapid development of computer technology, molecular simulation techniques have demonstrated their unique advantages in screening high-quality adsorbents for energy storage working pairs (Zhang et al., 2022; Lei et al., 2023). Currently, research on organic working pairs in nano-porous materials mostly focuses on the discussion of adsorption mechanisms and analysis of storage properties (Zhou et al., 2019; Li et al., 2020; Zheng et al., 2020; García et al., 2021). The reports on desorption processes and regeneration properties of MOHCs are few. Besides, for different heat source environments, there are multiple choices of working fluids for ORC. With the growing awareness of environmental protection, the fourth-generation refrigerants with low global warming potential (GWP) and zero ozone depletion potential (ODP) will gradually replace the existing third-generation refrigerants. Among them, R1234yf, R134a, R32 are currently the hot topics of research (Fouad and Vega, 2018; Liu et al., 2019). MOF-5 (Annapureddy et al., 2014), as a fundamental and classic MOF structure, exhibits good thermal stability and chemical stability at around 300°C, making it suitable for the application environment of low-grade energy in ORC systems. MOF-74 (Chaemchuen et al., 2018), being one of the MOFs with the highest unsaturated metal site density, can enhance its adsorption performance by adjusting the types of metal ions. Among the MOF-74 series, Co-MOF-74 stands out as the material with the maximum adsorption heat, gaining widespread attention.

Consequently, in this work, the metal-organic frameworks materials of MOF-5 and Co-MOF-74 are employed along with organic working fluids R32, R1234yf, R134a and their mixtures to form corresponding adsorption working pairs. Molecular dynamics simulations are conducted to investigate the desorption and regeneration behaviors of the organic working fluids within the MOFs. This work also aims to provide useful insight in adsorption refrigeration.

TABLE 1 The molar ratio of mixed refrigerants.

Mixed refrigerants	molar ratio
R1234yf + R32	1:3
R1234yf + R32	1:1
R1234yf + R32	3:1
R134a + R32	1:3
R134a + R32	1:1
R134a + R32	3:1

2 Methodology

2.1 Simulation models

This study simulated the adsorption and desorption regeneration processes of pure refrigerants (R1234yf, R134a, R32) and their mixtures (Table 1) within MOF-5 and Co-MOF-74.

The spatial structures of MOF-5 (Fig. a) and Co-MOF-74 (Fig. b) were shown in Figure 1. The MOF-5 adopts a 2 × 2 × 2 supercell structure (X: 5.1664 nm, Y: 5.1664 nm, Z: 5.1664 nm). It consists of 1536 C atoms, 768 H atoms, 832 O atoms, and 256 Zn atoms. Besides, the Co-MOF-74 utilizes a 1 × 1 × 4 supercell structure (X: 2.6136 nm, Y: 2.6136 nm, Z: 2.7768 nm). It contains 288 C atoms, 72 H atoms, 216 O atoms, and 72 Co atoms. The atomic partial charges for the MOF materials were calculated by the Extended Charge Equilibration (EQeq) method (Wilmer et al., 2012). The interatomic interactions were described by the 12–6 Lennard-Jones (LJ) potential (Xu et al., 2019). Specific force field parameters were listed in Table 2.

The molecular structures of the three selected organic working fluids in this study are illustrated in Figure 2. A full atomistic force field model, proposed by Raabe and Maginn (Raabe and Maginn, 2010), was employed to investigate these organic working fluids. The potential energy of interparticle interactions can be described by Eq. 1:

$$U = \sum_{bonds} k_d (d - d_0)^2 + \sum_{angles} k_\varphi (\varphi - \varphi_0)^2 + \sum_{dihedral} k_\chi [1 + \cos(n\chi - \delta)] + \sum_i \sum_{i<j} \left\{ 4\varepsilon_{ij} \left[\left(\frac{\sigma_{ij}}{d_{ij}} \right)^{12} - \left(\frac{\sigma_{ij}}{d_{ij}} \right)^{6} \right] + \frac{1}{4\pi\varepsilon_0} \frac{q_i q_j}{d_{ij}} \right\} \quad (1)$$

Furthermore, the cutoff distance for intermolecular interactions was set to 12 Å. The non-bonded interaction parameters between different types of atoms were calculated by the Lorentz-Berthelot combination rules (Delhommelle and MilliÉ, 2001). The particle-particle/particle-mesh (PPPM) method (Hockney et al., 1974) was employed to calculate the long-range Coulomb interactions.

The initial model for adsorption simulation is shown in Figure 3A (R1234yf/MOF-5). The model consisted of a 2 × 2 × 2 supercell of MOF-5 and two liquid membrane of R1234yf. The simulation box size was X: 53.355 Å, Y: 53.355 Å, Z: 181.134 Å. Each liquid membrane consisted of 648 R1234yf molecules distributed on both sides of the simulation box with dimensions of X: 53.355 Å, Y: 53.355 Å and Z: 34.80 Å. The MOF-5 supercell was positioned in the

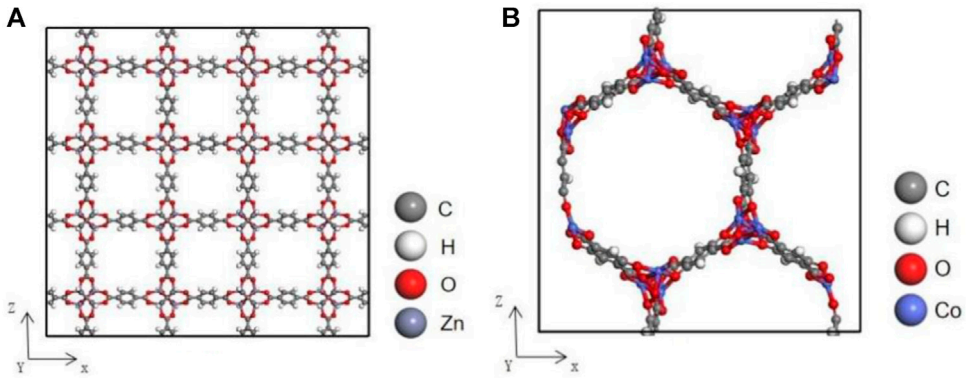

FIGURE 1
Structures of MOFs: **(A)** MOF-5 2 × 2×2 supercell; **(B)** Co-MOF-74 1 × 1×4 supercell.

TABLE 2 The force field parameters used for MOF-5 and Co-MOF-74.

Parameter	MOF-Zn	MOF-C	MOF-O	MOF-H	MOF-Co
σ (Å)	2.462	3.431	3.118	2.571	2.560
ε/k_B (K)	62.40	52.84	30.19	22.14	7.045

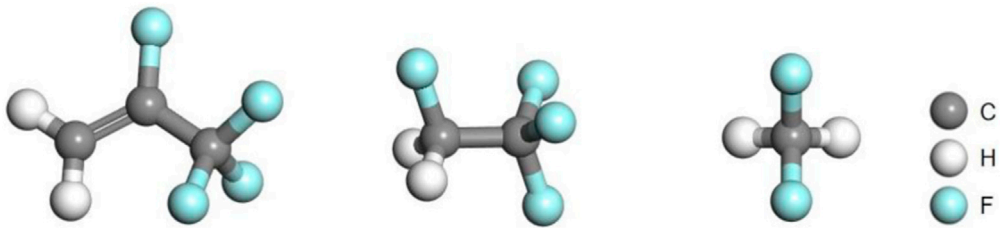

FIGURE 2
Spatial structures of R1234yf, R134a and R32.

center of the system along the Z direction and accounts for 25% mass fraction in the entire system. Periodic boundary conditions were applied in all three directions for the simulation box. The initial model for desorption regeneration was obtained by removing the unabsorbed working fluids outside the MOF from the model at the end of adsorption at 300 K, as shown in Figure 3B.

2.2 Simulation details

In this study, the molecular dynamics simulation processes were conducted by the Large-scale Atomic/Molecular Massively Parallel Simulator (LAMMPS) (Plimpton, 1995). The visualization of the models and research processes were performed with the OVITO software (Alexander, 2010). The thermophysical data for the organic working fluids were obtained from the National Institute of Standards and Technology (NIST) (webbook). The entire simulation processes were carried out under the NVT canonical ensemble. And the adsorption temperatures were set at 300 K, 330 K, 360 K, and 390 K, and the desorption temperatures were set at 330 K, 360 K, and 390 K. The Berendsen thermostat method (Berendsen et al., 1984) was utilized to control the system temperature. The time step was set at 1 fs with adsorption and desorption simulations performed at each temperature for 5 ns. Atom information was output every 10,000 steps.

3 Analysis of the adsorption process

To validate the accuracy of the computational model utilized in this study, the adsorption capacity of R134a in MOF-5 was simulated. The adsorption capacity of R134a in MOF-5 at 330 K of present model is about 1.442 g/g while that of previous work (Liu et al., 2022) is about 1.405 g/g, yielding a relative error of 2.5%. Thus, the utilization of the computational model in investigating the adsorption and desorption processes of organic working fluids in metal-organic framework materials is deemed feasible in this study.

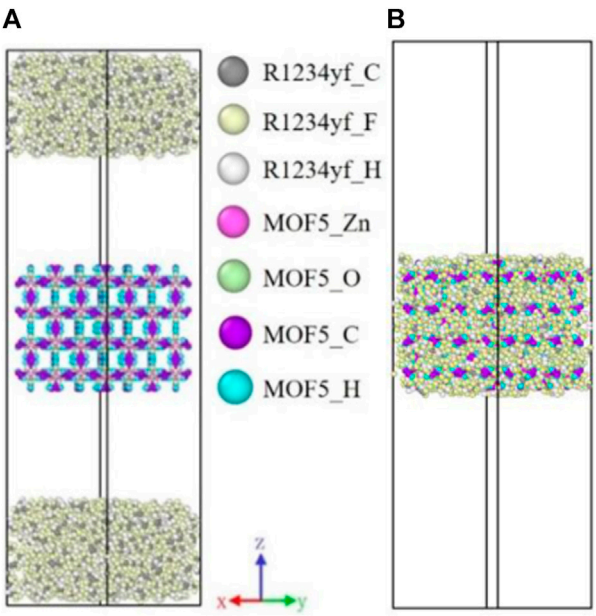

FIGURE 3
The initial model of adsorption and desorption of the R1234yf/MOF-5 working pair system. **(A)** adsorption; **(B)** desorption.

3.1 Adsorption capacity

The molecules of working fluid located in the region of MOFs are regarded as the adsorbed particles, which is used for calculating the adsorption capacities, $m_{adsorption}$, and its specific calculation formula (2) is as follows:

$$m_{adsorption} = \frac{n_{fluid} \cdot m_{fluid}}{M_{MOF}} \quad (2)$$

The adsorption capacities of pure working fluids, including R1234yf, R134a, R32, as well as their mixed counterparts in MOF-5, are statistically analyzed and are presented in Figure 4. The results show that a decrease in adsorption capacity with increasing temperature for both pure and mixed working fluids, which agree with previous related works (Hu et al., 2018a; Hu et al., 2018b; Hu et al., 2019; Liu et al., 2022). This can be attributed to the increase in thermodynamic energy of the working fluid and the enhancement of molecular thermal motion caused by temperature increase, leading to facilitating desorption of organic working fluids from the surface of porous materials. In terms of adsorption capacity for pure working fluids, the ranking order is R134a > R1234yf > R32.

And the analysis of adsorption data for mixed refrigerants reveals that in the adsorption of mixed refrigerants, the adsorption capacities of each component are lower than the pure refrigerants. This is attributed to the shared occupancy of the MOF-5 internal space by the mixed refrigerants. Among the three organic refrigerants, R1234yf and R134a have similar sizes, both larger than R32. The similar phenomenon is also can be found in Li et al. work (Li et al., 2020). Due to the smaller pore size of MOF-5, R1234yf and R134a occupy the majority of the adsorption sites, which results in a significant decrease in the adsorption capacity of R32. As the quantity of R1234yf and R134a increases, the decrease in the adsorption capacity of R32 becomes more pronounced. Additionally, the adsorption capacity of R1234yf in R1234yf/R32 is higher than that of R134a in R134a/R32, which is contrary to the results obtained for pure refrigerants. This is due to the stronger adsorption selectivity of R1234yf towards R32 compared to R134a during the adsorption of mixed refrigerants. The observation is further supported by the higher adsorption capacity of R32 in R134a/R32 compared to R1234yf/R32. When the molar ratio of R1234yf to R32 is 2:1 in R1234yf/R32, the adsorption capacity exceeds that of the individual pure refrigerant components. This is attributed to the utilization of the MOF-5 pore space through the combination of the large molecular structure of R1234yf and the small molecular structure of R32 at the current molar ratio, which is resulting in superior performance compared to pure refrigerants.

The adsorption amounts of organic refrigerants in Co-MOF-74 are shown in Figure 5. Similar to MOF-5, the adsorption amounts of organic refrigerants decrease with the increase of temperature. The relationship among the adsorption amounts of pure refrigerants is as follows: R134a > R1234yf > R32.

The analysis of the adsorption data for mixed refrigerants reveals that in the adsorption of mixed refrigerants, the adsorption capacities of each component are lower than those of pure refrigerants. This can be attributed to the shared occupancy of the Co-MOF-74 internal space by the mixed refrigerants. In the case of R1234yf/R32 and R134a/R32 mixed refrigerants with a molar ratio of 2:1, both R1234yf and R134a exhibit an increase in adsorption amount with increasing temperature. This is due to the enhanced molecular thermal motion at higher temperatures, which makes it easier for the smaller-sized R32 molecules to desorb from the porous material, which creates vacant adsorption sites for a small amount of R1234yf and R134a molecules to enter.

In the R134a/R32 mixed refrigerant system, the adsorption amount of R134a is higher than that of R1234yf in the R1234yf/R32 mixed refrigerant. This indicates that during the adsorption of mixed refrigerants in Co-MOF-74, R134a exhibits stronger adsorption selectivity towards R32 compared to R1234yf. When the molar ratio of R1234yf to R32 is 2:1 in the R1234yf/R32 mixed refrigerant, the adsorption amount exceeds that of the individual pure refrigerant components. This is attributed to the effective utilization of the Co-MOF-74 pore space through the combination of the large molecular structure of R1234yf and the small molecular structure of R32 at the current molar ratio, which results in superior performance compared to pure refrigerants.

Next, the adsorption capacity of organic working fluids in two different metal-organic framework (MOF) materials, MOF-5 and Co-MOF-74, was analyzed. It was observed that, for different organic working fluids, the adsorption capacity followed the trend of MOF-5>Co-MOF-74. This can be attributed to the distinct structural characteristics of the two MOF materials. MOF-5, with its three-dimensional network structure, exhibits a larger specific surface area and higher porosity compared to Co-MOF-74, which possesses a three-dimensional structure with one-dimensional pore channels. A larger specific surface area and higher porosity result in more available adsorption sites per unit mass of the MOFs, leading to a higher adsorption capacity of organic working fluids.

Furthermore, in the adsorption of mixed working fluids in MOF-5, it was observed that the adsorption capacity of R1234yf

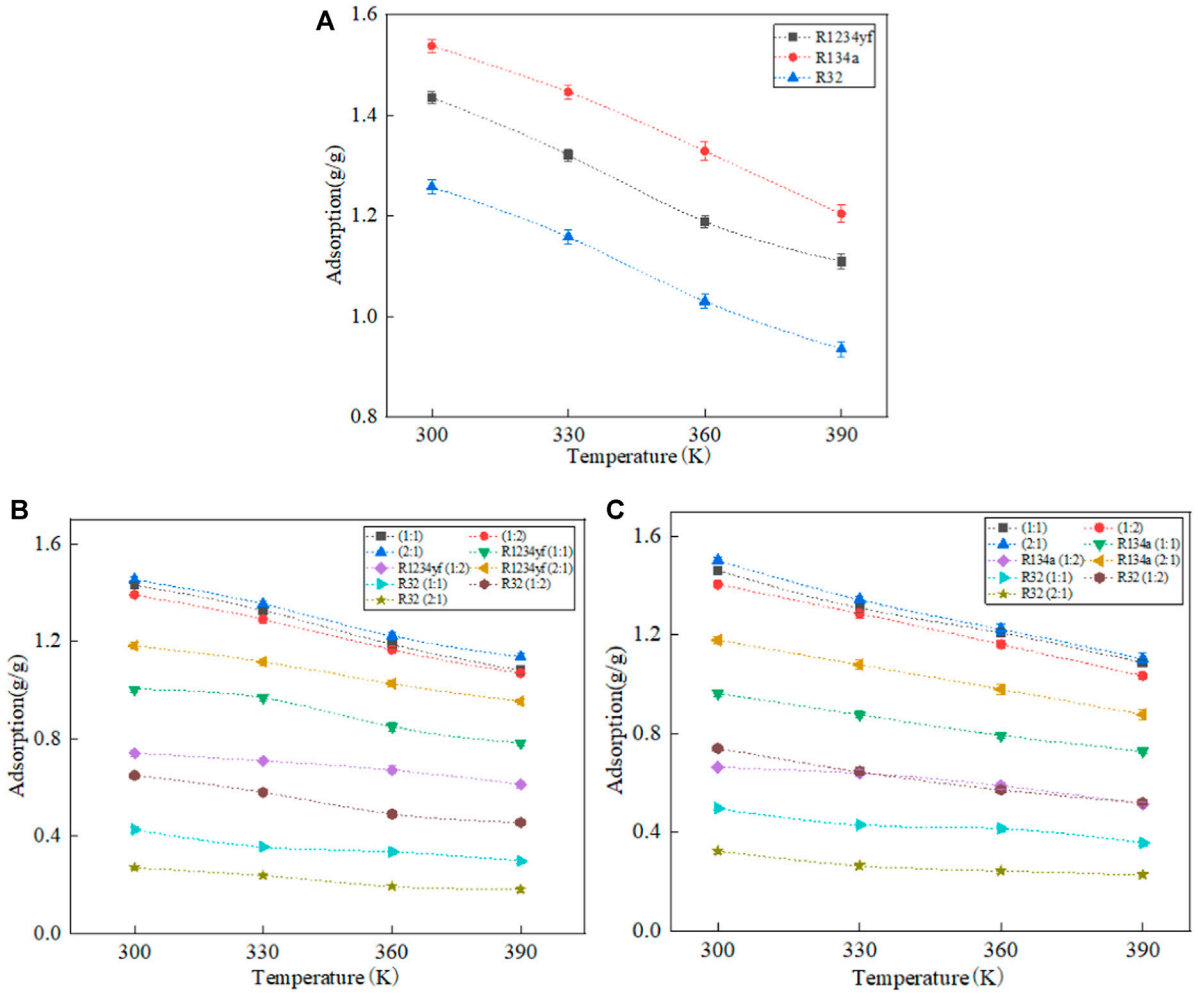

FIGURE 4
Adsorption of pure working fluids and their mixtures in MOF-5. **(A)** pure working fluids, **(B)** R1234yf/R32, **(C)** R134a/R32.

in the R1234yf/R32 mixture was higher than that of R134a in the R134a/R32 mixture. However, in Co-MOF-74, the opposite trend was observed. This discrepancy can be attributed to the smaller pore size of MOF-5, where R1234yf, being the largest molecule among the three working fluids, occupies a majority of the available space, resulting in a higher adsorption capacity. On the other hand, Co-MOF-74 has a larger pore size, and the size of the organic working fluid molecules has a lesser impact on the adsorption capacity. As a result, the pure working fluid with the highest adsorption capacity, R134a, exhibits a higher adsorption capacity in Co-MOF-74. Additionally, the smaller pore size of MOF-5 also prevents the phenomenon of increasing adsorption capacity of mixed working fluid components with rising temperature, which is observed in Co-MOF-74.

3.2 Adsorption heat

Adsorption heat is the thermal effect generated during the adsorption process of a substance and serves as an important indicator of adsorption characteristics. During the adsorption process, gas or liquid molecules move towards the surface of the porous medium, leading to a significant decrease in their thermodynamic energy. This energy is converted into surface energy, releasing heat, which is known as adsorption heat. The adsorption heat can be calculated using the following equation (3) (Niu et al., 2019):

$$\Delta E = E_{adsorbent} + E_{adsorbate} - E_{adsorbent+adsorbate} \quad (3)$$

where $E_{adsorbent+adsorbate}$ represents the energy of the stable configuration formed between the organic adsorbate and the metal-organic framework material. $E_{adsorbent}$ represents the energy of the metal-organic framework material before adsorption, and $E_{adsorbate}$ represents the energy of the organic adsorbate before adsorption. ΔE is the adsorption heat. Since the adsorption process typically releases heat, a larger ΔE indicates a greater amount of heat released during the adsorption process, resulting in a more stable configuration after adsorption.

The adsorption heat of organic working fluids in MOF-5 is shown in Figure 6. At about 330 K, the adsorption heat suddenly increases, which is attributed to a phase transition of the organic working fluid at this temperature, leading to an increase in $E_{adsorbate}$.

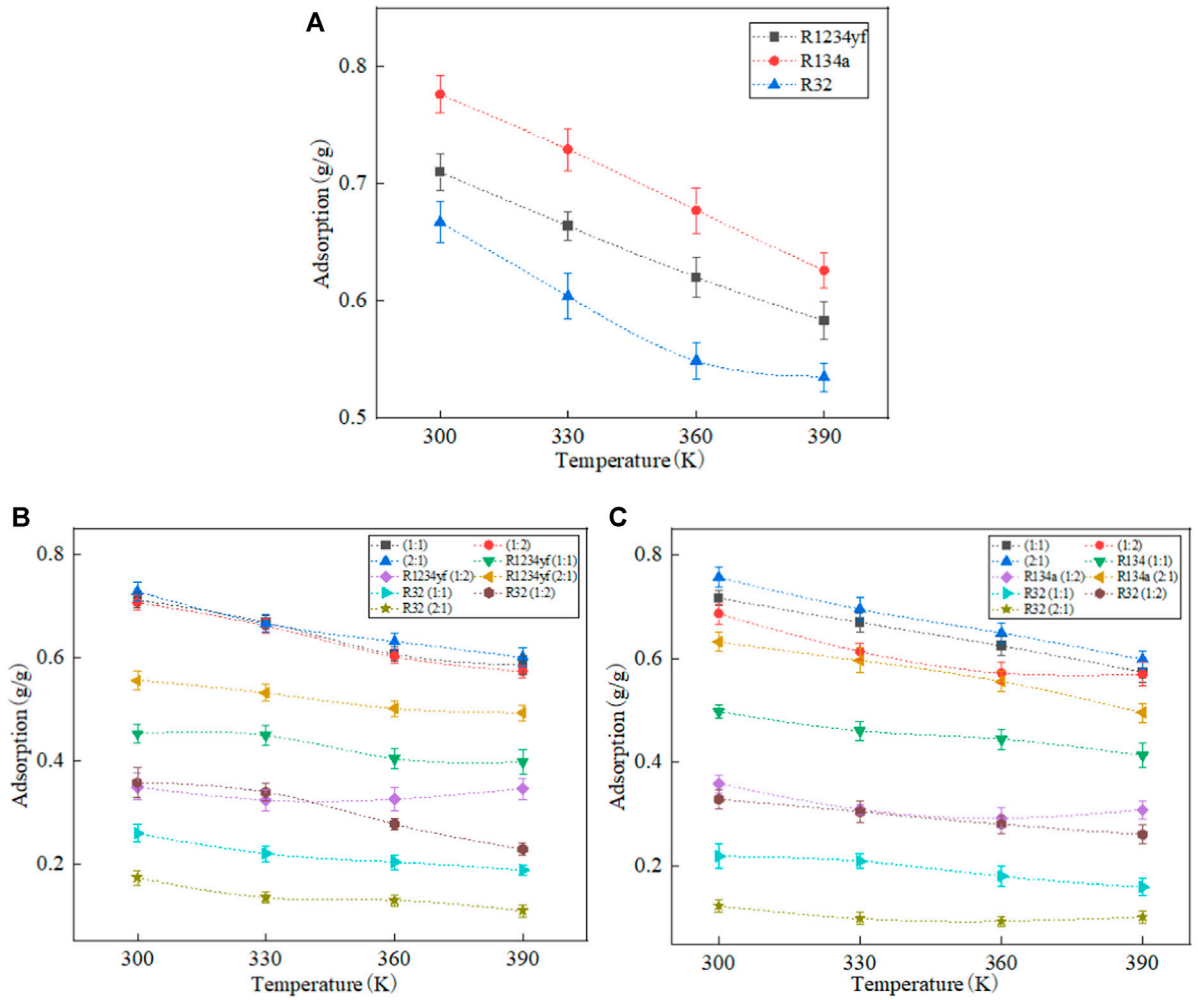

FIGURE 5
Adsorption of pure working fluids and their mixtures in Co-MOF-74. **(A)** pure working fluids, **(B)** R1234yf/R32, **(C)** R134a/R32.

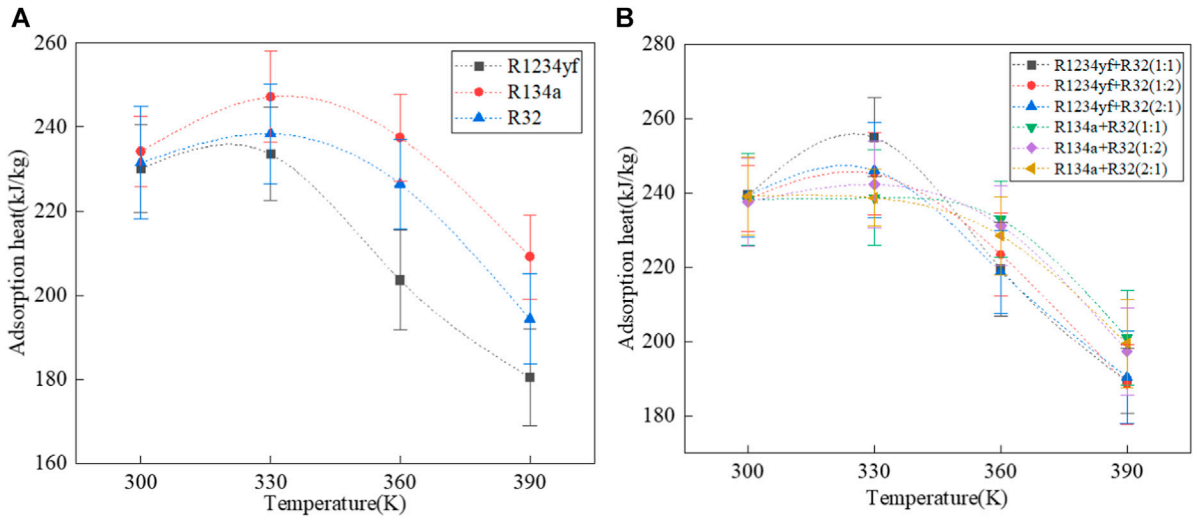

FIGURE 6
Adsorption heat of pure and mixed working fluids in MOF-5. **(A)** pure working fluids, **(B)** mixed working fluids.

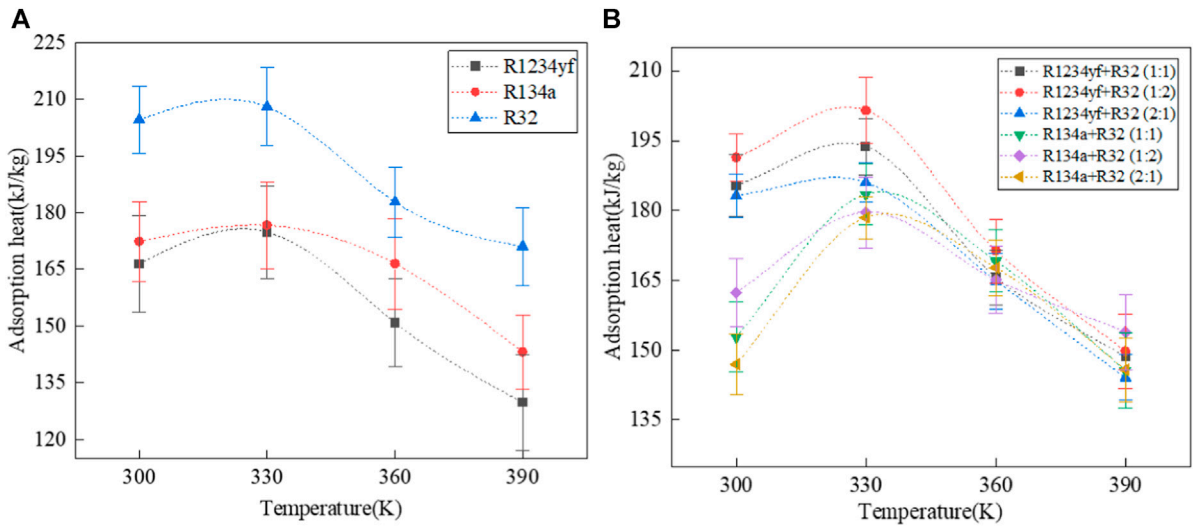

FIGURE 7
Adsorption heat of pure and mixed working fluids in Co-MOF-74. **(A)** pure working fluids. **(B)** mixed working fluids.

Apart from the phase transition point, as the temperature rises, the adsorption of organic working fluids per unit mass of the MOF decreases, and the adsorption heat also decreases accordingly. The magnitude of adsorption heat for pure working fluids in MOF-5 follows the order: R134a > R32 > R1234yf. The higher the proportion of fluorine atoms, the greater the adsorption heat, possibly due to the stronger interaction forces between the fluorine atoms and other atoms during adsorption.

The adsorption heat curve of mixed working fluids is more complex compared to pure working fluids, which is due to the presence of multiple components in the mixture. During adsorption, although the adsorption amount decreases with the increase of temperature, the changes in composition vary due to different adsorption selectivity. Overall, the adsorption heat of the R134a/R32 mixed working fluid is higher than that of the R1234yf/R32 mixed working fluid. This is partly because the adsorption heat of pure R134a is greater than that of R1234yf. Additionally, R1234yf exhibits stronger adsorption selectivity in MOF-5, resulting in a lower adsorption amount of R32 in the R1234yf/R32 mixed working fluid compared to the adsorption amount of R32 in the R134a/R32 mixed working fluid.

The adsorption heats of organic adsorbates in Co-MOF-74 are shown in Figure 7. Similar to MOF-5, there is a sharp transition point due to phase change in the adsorption heat at 330 K, and the overall adsorption heat decreases with increasing temperature. The order of adsorption heats for pure adsorbates in Co-MOF-74 is R32 > R134a > R1234yf, which is different from that in MOF-5 where the order is R134a > R32 > R1234yf. This is partly because the mass fractions of fluorine in R32 (73.07%) and R134a (74.50%) are similar, and partly because the difference in adsorption between R32 and R134a in Co-MOF-74 is smaller than that in MOF-5.

The adsorption heat of R1234yf/R32 mixed refrigerant is higher than that of R134a/R32 mixed refrigerant, because the adsorption of R32 in R1234yf/R32 mixed refrigerant is greater than that in R134a/R32 mixed refrigerant. In addition, in both types of mixed refrigerants, the order of adsorption heats is 1:2 M ratio >1:1 M ratio >2:1 M ratio. That is, the adsorption heat of mixed refrigerants is proportional to the mass fraction of R32.

Then, the comparative analysis of the adsorption heats of organic adsorbates in two types of MOF materials reveals that for different organic adsorbates, the order of adsorption heats is consistently MOF-5 > Co-MOF-74. Therefore, it can be concluded that for the same adsorbate at the same temperature, its adsorption heat in a unit mass of MOF is directly proportional to the specific surface area and porosity of the MOF material. The adsorption heat increases when the organic adsorbate undergoes phase transition, and generally decreases with increasing temperature. On the other hand, for mixed refrigerants, although the adsorption capacity decreases with increasing temperature, the variation in composition differs due to different adsorption selectivity. This complexity results in a more intricate adsorption heat curve. Overall, for mixed refrigerants with the same composition, the adsorption heat increases with an increase in the mass fraction of the component with higher adsorption heat.

4 Analysis of the desorption process

4.1 Desorption regeneration rate

After completing the adsorption process in MOFs, the accumulated organic refrigerants within them need to undergo a desorption regeneration process to achieve the recycling of the adsorbent. Therefore, the regenerability of the refrigerant in MOFs is a key indicator during the desorption process. Due to variations in the initial adsorption amounts among different adsorption models, it is not appropriate to simply use the desorption amount as a measure of the regenerability of organic refrigerants in MOFs. In this study, the desorption regeneration rate is employed to evaluate the regenerability of organic refrigerants. The desorption regeneration rate is defined as the ratio of the

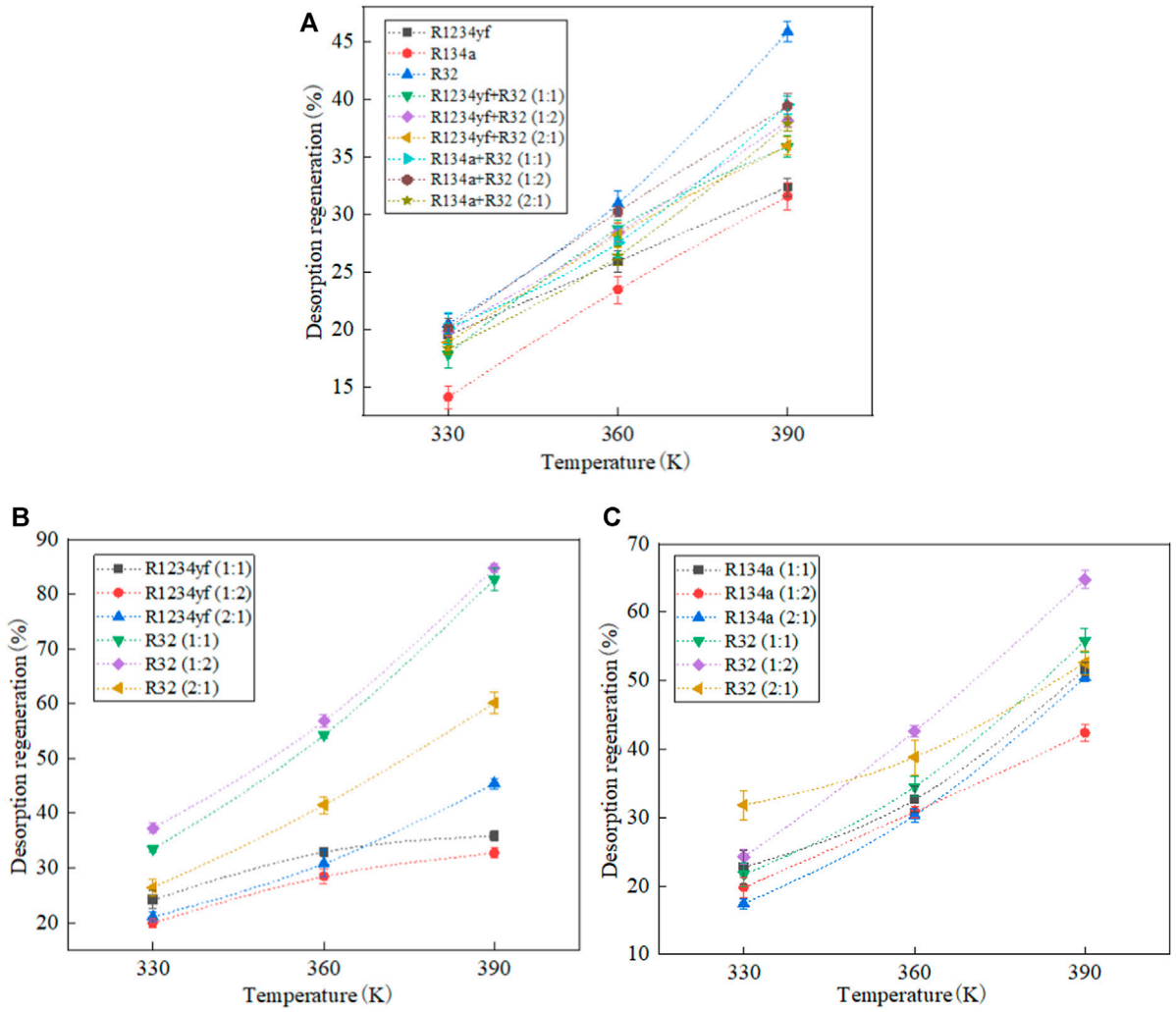

FIGURE 8
Desorption regeneration rates of pure and mixed working fluids in MOF-5. **(A)** desorption and regeneration rates of each organic working fluid, **(B)** R1234yf/R32, **(C)** R134a/R32.

desorption amount to the original adsorption amount, which can be calculated using Eq. (4):

$$R_{desorption} = \left(1 - \frac{n_{T1}}{n_{T0}}\right) \times 100\% \quad (4)$$

where n_{T0} and n_{T1} are the moles of working fluids in the MOF at adsorption and desorption temperature, respectively.

The desorption regeneration rates of organic refrigerants and their mixtures in MOF-5 are shown in Figure 8. As the temperature increases, the desorption regeneration rate also increases. The reason for this phenomenon is that with the temperature rising, the thermodynamic energy of the organic refrigerant molecules increases, which makes them more likely to desorb from the MOF. The desorption regeneration rates of pure refrigerants are in the following order: R32 > R1234yf > R134a. This is due to the smaller size of R32 molecules which makes them easier to desorb from the MOF. R1234yf and R134a have similar molecular sizes, but R134a exhibits stronger interactions with MOF-5, which results in a slightly lower desorption regeneration rate compared to R1234yf.

Among mixtures of the same composition but different molar ratios, the desorption regeneration rate is directly proportional to the mass fraction of R32. The order of desorption regeneration rates is as follows: molar ratio (1:2) > molar ratio (1:1) > molar ratio (2:1). For mixtures with the same molar ratio but different components, the order of desorption regeneration rates is R134a/R32 > R1234yf/R32. This is because the adsorption amount of R32 varies in different mixtures. During adsorption, R1234yf exhibits stronger selectivity for R32 compared to R134a. The adsorption amount of R32 in R134a/R32 is greater than that in R1234yf/R32, which results in a higher desorption regeneration rate for R134a/R32 compared to R1234yf/R32.

Analyzing the desorption regeneration rates of each component in the mixture, it is observed that the desorption regeneration rate of R32 is not only greater than the other components but also higher than the desorption regeneration rate of the pure refrigerant. This finding indicates that the intermolecular interactions between different molecular species in the mixture play a promoting role in the desorption process.

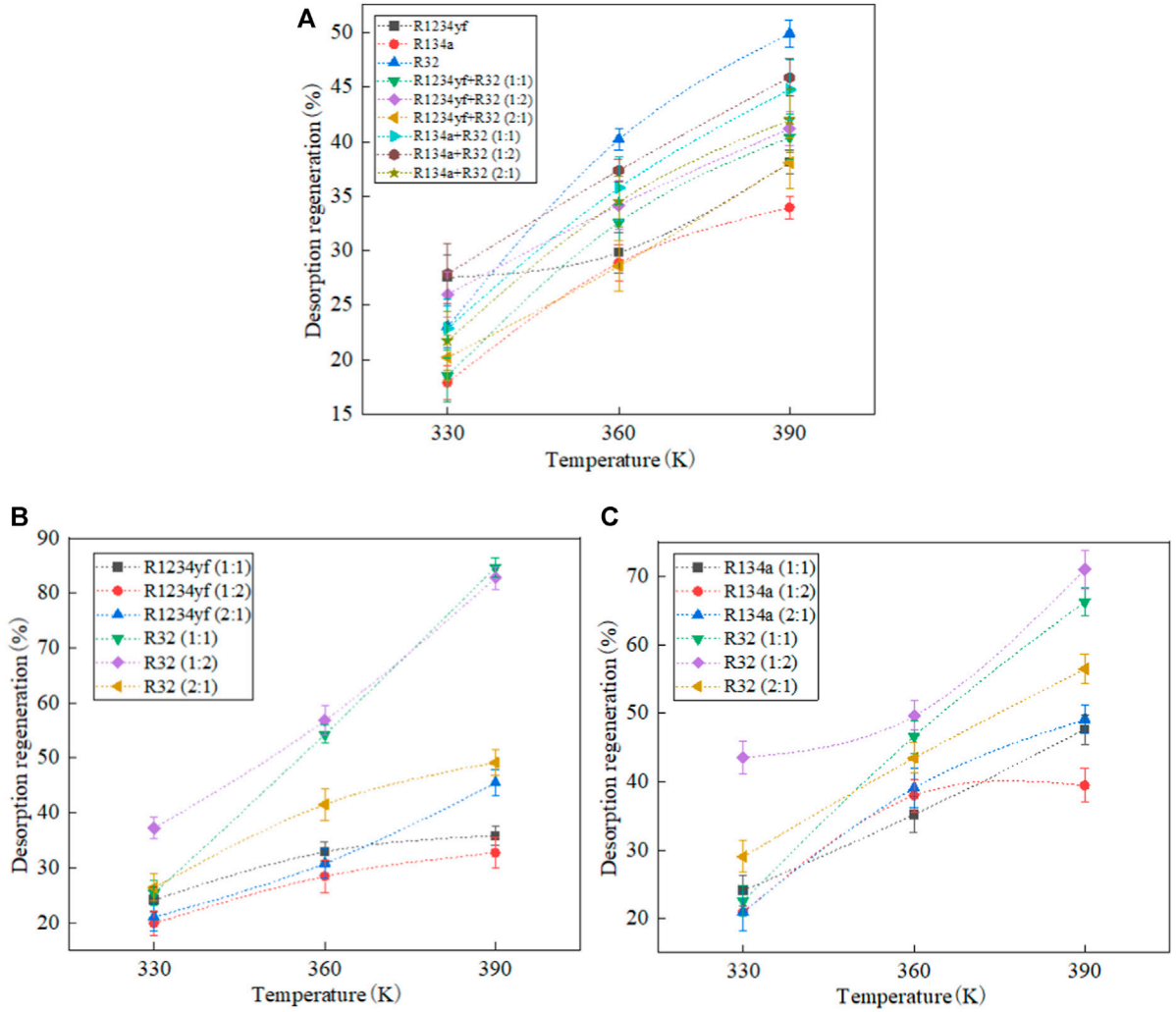

FIGURE 9
Desorption regeneration rates of pure and mixed working fluids in Co-MOF-74. **(A)** desorption and regeneration rates of each organic working fluid, **(B)** R1234yf/R32, **(C)** R134a/R32.

The desorption regeneration rates of organic refrigerants in Co-MOF-74 are shown in Figure 9. As the temperature increases, the desorption regeneration rate also increases. The order of desorption regeneration rates of pure refrigerants is the same as that in MOF-5, namely, R32 > R1234yf > R134a. For mixtures with the same composition but different molar ratios, the desorption regeneration rate is directly proportional to the mass fraction of R32. The order of desorption regeneration rates is molar ratio (1:2) > molar ratio (1:1) > molar ratio (2:1). For mixtures with the same molar ratio but different components, the order of desorption regeneration rates is R134a/R32 > R1234yf/R32.

Besides, it is found that R32 which has a smaller molecular structure exhibits a higher desorption regeneration rate than the other components in the mixture. Due to the intermolecular interactions between different molecular species in the mixture, the desorption regeneration rates of each component in the mixture are higher than those of their corresponding pure refrigerants. And for the same organic working fluid, the desorption regeneration rate follows the order Co-MOF-74 > MOF-5. This is attributed to the different structures of the MOFs. Co-MOF-74, as a one-dimensional porous metal-organic framework material with a three-dimensional structure, has larger pore size and simpler internal structure compared to MOF-5, making it easier for organic working fluids to desorb.

4.2 Desorption heat

Desorption heat refers to the thermal effect generated during the desorption process of a working fluid. Here, desorption heat is defined as the energy released per unit mass of MOF during the desorption process of the organic working fluid, starting from the system state when the adsorption of the working fluid ends at 300 K. This can be obtained by calculating the energy difference before and after the desorption process using a simulation model, the specific calculation method is shown in Eq. (5):

$$\Delta E = E_{adsorbent+adsorbate} - (E_{adsorbent} + E_{adsorbate}) \quad (5)$$

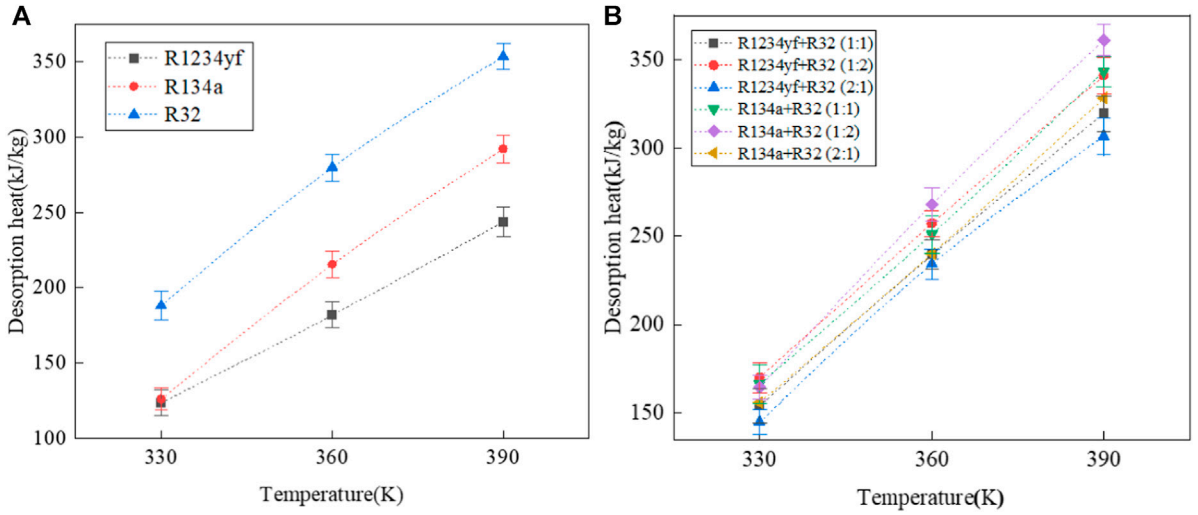

FIGURE 10
Desorption heat of pure and mixed working fluids in MOF-5. **(A)** pure working fluids, **(B)** mixed working fluids.

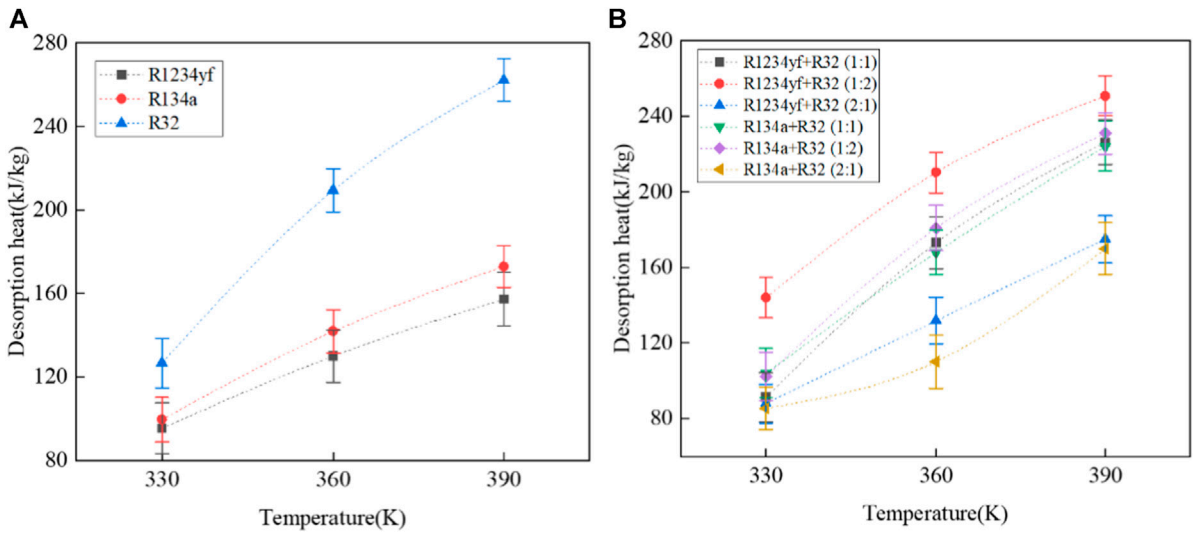

FIGURE 11
Desorption heat of pure and mixed working fluids in Co-MOF-74. **(A)** pure working fluids, **(B)** mixed working fluids.

where $E_{adsorbent+adsorbate}$ is the energy of the stable configuration formed by the adsorption working pairs. $E_{adsorbent}$ denotes the energy after desorption of MOF, $E_{adsorbate}$ is the energy of working fluids after desorption.

The desorption heats of pure adsorbates and their mixed refrigerants in MOF-5 are shown in Figure 10. It can be observed that as the temperature increases, both the desorption heats of pure adsorbates and mixed refrigerants increase. This is because at higher temperatures, more organic fluid adsorbates are released from the MOF, resulting in the release of more heat. For pure adsorbates, the order of desorption heats is R32 > R134a > R1234yf, which is inversely proportional to the molecular volume of the organic adsorbates.

For mixed refrigerants with the same composition but different molar ratios, the relationship between desorption heats follows the order: molar ratio (1:2) > molar ratio (1:1) > molar ratio (2:1). In other words, for mixed refrigerants with the same composition, the desorption heat increases as the mass fraction of R32 in the mixed refrigerant increases. As for mixed refrigerants with the same molar ratio but different components, the relationship between desorption heats follows the order: R134a > R1234yf, which similarly aligns with the conclusion that desorption heat is inversely proportional to the molecular volume of the organic adsorbates.

The desorption heats of pure refrigerants and their mixed refrigerants in Co-MOF-74 are shown in Figure 11. As the temperature increases, the desorption heat also increases. In the

desorption process of pure refrigerants, R32 exhibits the highest desorption heat, reaching 262.27 kJ/kg at 390 K, while R1234yf exhibits the lowest desorption heat, with a value of 157.31 kJ/kg at 390 K.

For mixed refrigerants with the same composition but different molar ratios, the desorption heat increases as the mass fraction of R32 in the mixed refrigerant increases, following the order: molar ratio (1:2) > molar ratio (1:1) > molar ratio (2:1). As for mixed refrigerants with the same molar ratio but different components, the relationship between desorption heats follows the order: R1234yf > R134a.

Besides, for the same working fluid, the desorption heat in MOF-5 is greater than that in Co-MOF-74. Hence, desorption heat exhibits a similar relationship to adsorption amount and heat, increasing with higher specific surface area and porosity. The order of desorption heats for pure working fluids in both MOF materials is as follows: R32 > R134a > R1234yf. For mixed working fluids with the same composition, the desorption heat increases with the mass fraction of R32 in the mixture. In Co-MOF-74, the desorption heat varies significantly with changes in molar ratio for mixed working fluids.

5 Conclusion

This work investigates the adsorption and desorption regeneration processes of pure refrigerants R1234yf, R134a, R32, and their mixtures in MOF-5 and Co-MOF-74 through simulation. The following conclusions can be drawn,

(1) The adsorption capacity of organic refrigerants is inversely proportional to temperature. The mixed refrigerant R1234yf/R32 (with a molar ratio of 2:1) fully utilizes the space within the MOF, resulting in a higher adsorption capacity compared to the individual pure components.
(2) When organic refrigerants undergo phase transitions, their adsorption heat suddenly increases due to the increased thermodynamic potential of the refrigerant itself. In the absence of phase transitions, the adsorption heat decreases with increasing temperature.
(3) With the increase in temperature, the thermal motion capability of molecules enhances, resulting in higher desorption capacity, desorption regeneration rate, and desorption heat of organic refrigerants in the MOF material.
(4) Co-MOF-74 with larger pore size exhibits a higher desorption regeneration rate than MOF-5, while MOF-5 has a higher desorption heat compared to Co-MOF-74.
(5) R32 is more easily desorbed from the MOF material with smaller molecular structure. The interactions between atoms of different molecules in the mixed refrigerant play a promoting role in the desorption process.

Data availability statement

The raw data supporting the conclusion of this article will be made available by the authors, without undue reservation.

Author contributions

XC: Writing–original draft.

Funding

The author(s) declare that no financial support was received for the research, authorship, and/or publication of this article.

Conflict of interest

The author declares that the research was conducted in the absence of any commercial or financial relationships that could be construed as a potential conflict of interest.

Publisher's note

References

Alexander, S. (2010). Visualization and analysis of atomistic simulation data with OVITO–the Open Visualization Tool. *Model. Simul. Mater. Sci. Eng.* 18 (1), 015012. doi:10.1088/0965-0393/18/1/015012

Annapureddy, H. V. R., Motkuri, R. K., Nguyen, P. T., Truong, T. B., Thallapally, P. K., McGrail, B. P., et al. (2014). Computational studies of adsorption in metal organic frameworks and interaction of nanoparticles in condensed phases. *Mol. Simul.* 40 (7-9), 571–584. doi:10.1080/08927022.2013.829224

Berendsen, H. J. C., Postma, J. P. M., van Gunsteren, W. F., DiNola, A., and Haak, J. R. (1984). Molecular dynamics with coupling to an external bath. *J. Chem. Phys.* 81 (8), 3684–3690. doi:10.1063/1.448118

Carbon (2021). Project team on the strategy and pathway for peaked carbon emissions and carbon neutrality. Analysis of a peaked carbon emission pathway in China toward carbon neutrality. *Engineering* 7 (12), 1673–1677. doi:10.1016/j.eng.2021.10.003

Chaemchuen, S., Xiao, X., Klomkliang, N., Yusubov, M., and Verpoort, F. (2018). Tunable metal–organic frameworks for heat transformation applications. *Nanomaterials* 8 (9), 661. doi:10.3390/nano8090661

Chen, X., Liu, C., Li, Q., Wang, X., and Xu, X. (2019). Dynamic analysis and control strategies of Organic Rankine Cycle system for waste heat recovery using zeotropic mixture as working fluid. *Energy Convers. Manag.* 192, 321–334. doi:10.1016/j.enconman.2019.04.049

Delhommelle, J., and MilliÉ, P. (2001). Inadequacy of the Lorentz-Berthelot combining rules for accurate predictions of equilibrium properties by molecular simulation. *Mol. Phys.* 99 (8), 619–625. doi:10.1080/00268970010020041

Fouad, W. A., and Vega, L. F. (2018). Next generation of low global warming potential refrigerants: thermodynamic properties molecular modeling. *AIChE J.* 64 (1), 250–262. doi:10.1002/aic.15859

Furukawa, H., Cordova, K. E., O'Keeffe, M., and Yaghi, O. M. (2013). The chemistry and applications of metal-organic frameworks. *Science* 341 (6149), 1230444. doi:10.1126/science.1230444

García, E. J., Bahamon, D., and Vega, L. F. (2021). Systematic search of suitable metal–organic frameworks for thermal energy-storage applications with low global warming potential refrigerants. *ACS Sustain. Chem. Eng.* 9 (8), 3157–3171. doi:10.1021/acssuschemeng.0c07797

Hockney, R. W., Goel, S. P., and Eastwood, J. W. (1974). QUIET HIGH-RESOLUTION COMPUTER MODELS OF A PLASMA. *J. Of Comput. Phys.* 14 (2), 148–158. doi:10.1016/0021-9991(74)90010-2

Hu, J., Liu, C., Li, Q., and Liu, L. (2019). Thermal energy storage of R1234yf/MOF-5 and R1234ze(Z)/MOF-5 nanofluids: a molecular simulation study. *Energy Procedia* 158, 4604–4610. doi:10.1016/j.egypro.2019.01.870

Hu, J., Liu, C., Li, Q., and Shi, X. (2018a). Molecular simulation of thermal energy storage of mixed CO2/IRMOF-1 nanoparticle nanofluid. *Int. J. Heat Mass Transf.* 125, 1345–1348. doi:10.1016/j.ijheatmasstransfer.2018.04.162

Hu, J., Liu, C., Liu, L., and Li, Q. (2018b). Thermal energy storage of R1234yf, R1234ze, R134a and R32/MOF-74 nanofluids: a molecular simulation study. *Materials* 11 (7), 1164. doi:10.3390/ma11071164

Kong, X., Deng, H., Yan, F., Kim, J., Swisher, J. A., Smit, B., et al. (2013). Mapping of functional groups in metal-organic frameworks. *Science* 341 (6148), 882–885. doi:10.1126/science.1238339

Lei, G., Xi, G., Liu, Z., Li, Q., Cheng, H., and Liu, H. (2023). Enhancing selective adsorption of CO2 through encapsulating FeTPPs into Cu-BTC. *Chem. Eng. J.* 461, 141977. doi:10.1016/j.cej.2023.141977

Li, Q., Cai, S., and Liu, C. (2020). Molecular simulation of energy storage of R1234yf, R1234ze(z), R32, and their mixtures in Co-MOF-74 materials. *Chin. Sci. Bulletin-Chinese* 65 (7), 633–640. doi:10.1360/tb-2019-0435

Li, Q., Ren, J., Liu, Y., and Zhou, Y. (2022). Prediction of critical properties and boiling point of fluorine/chlorine-containing refrigerants. *Int. J. Refrig.* 143, 28–36. doi:10.1016/j.ijrefrig.2022.06.024

Liu, J., Cai, P., and Xu, H. (2022). Molecular simulation of energy storage properties of R32, R134A and R1234YF in MOF-5 AND MOF-177. *Int. J. Mod. Phys. B* 36 (01), 2250006. doi:10.1142/s0217979222500060

Liu, X., Wang, T., and He, M. (2019). Investigation on the condensation process of HFO refrigerants by molecular dynamics simulation. *J. Mol. Liq.* 288, 111034. doi:10.1016/j.molliq.2019.111034

McGrail, B. P., Thallapally, P., Blanchard, J., Nune, S., Jenks, J., and Dang, L. (2013). Metal-organic heat carrier nanofluids. *Nano Energy* 2 (5), 845–855. doi:10.1016/j.nanoen.2013.02.007

McLinden, M. O., and Huber, M. L. (2020). (R)Evolution of refrigerants. *J. Chem. Eng. Data* 65 (9), 4176–4193. doi:10.1021/acs.jced.0c00338

Miao, Z., Li, Z., Zhang, K., Xu, J., and Cheng, Y. (2020). Selection criteria of zeotropic mixtures for subcritical organic Rankine cycle based on thermodynamic and thermo-economic analysis. *Appl. Therm. Eng.* 180, 115837. doi:10.1016/j.applthermaleng.2020.115837

Niu, F. F., Cai, M., Pang, J., Li, X., Zhang, G., and Yang, D. (2019). A first-principles study: adsorption of small gas molecules on GeP3 monolayer. *Surf. Sci.* 684, 37–43. doi:10.1016/j.susc.2019.02.008

Plimpton, S. (1995). Fast parallel algorithms for short-range molecular dynamics. *J. Comput. Phys.* 117 (1), 1–19. doi:10.1006/jcph.1995.1039

Qasem, N. A. A., Ben-Mansour, R., and Habib, M. A. (2018). An efficient CO2 adsorptive storage using MOF-5 and MOF-177. *Appl. Energy* 210, 317–326. doi:10.1016/j.apenergy.2017.11.011

Raabe, G., and Maginn, E. J. (2010). Molecular modeling of the Vapor–Liquid equilibrium properties of the alternative refrigerant 2,3,3,3-Tetrafluoro-1-propene (HFO-1234yf). *J. Phys. Chem. Lett.* 1 (1), 93–96. doi:10.1021/jz900070h

Su, W., Zhao, L., and Deng, S. (2017). Recent advances in modeling the vapor-liquid equilibrium of mixed working fluids. *Fluid Phase Equilibria* 432, 28–44. doi:10.1016/j.fluid.2016.10.016

Vivian, J., Manente, G., and Lazzaretto, A. (2015). A general framework to select working fluid and configuration of ORCs for low-to-medium temperature heat sources. *Appl. Energy* 156, 727–746. doi:10.1016/j.apenergy.2015.07.005

Wang, P., Li, Q., Wang, S., He, C., and Wu, C. (2024). Off-design performance evaluation of thermally integrated pumped thermal electricity storage systems with solar energy. *Energy Convers. Manag.* 301, 118001. doi:10.1016/j.enconman.2023.118001

Wang, Q., Tang, S., and Li, L. (2018). Energy storage analysis of a mixed r161/MOF-5 nanoparticle nanofluid based on molecular simulations. *Materials* 11 (5), 848. doi:10.3390/ma11050848

Wang, S., Liu, C., Li, Q., Liu, L., Huo, E., and Zhang, C. (2020). Selection principle of working fluid for organic Rankine cycle based on environmental benefits and economic performance. *Appl. Therm. Eng.* 178, 115598. doi:10.1016/j.applthermaleng.2020.115598

Wang, S., Liu, C., Ren, J., Liu, L., Li, Q., and Huo, E. (2019). Carbon footprint analysis of organic rankine cycle system using zeotropic mixtures considering leak of fluid. *J. Clean. Prod.* 239, 118095. doi:10.1016/j.jclepro.2019.118095

webbook Available at: https://webbook.nist.gov/chemistry/

Wilmer, C. E., Kim, K. C., and Snurr, R. Q. (2012). An extended charge equilibration method. *J. Of Phys. Chem. Lett.* 3 (19), 2506–2511. doi:10.1021/jz3008485

Xiao, T., Liu, C., Wang, X., Wang, S., Xu, X., Li, Q., et al. (2022). Life cycle assessment of the solar thermal power plant integrated with air-cooled supercritical CO2 Brayton cycle. *Renew. Energy* 182, 119–133. doi:10.1016/j.renene.2021.10.001

Xu, G. J., Meng, Z., Guo, X., Zhu, H., Deng, K., Xiao, C., et al. (2019). Molecular simulations on CO2 adsorption and adsorptive separation in fullerene impregnated MOF-177, MOF-180 and MOF-200. *Comput. Mater. Sci.* 168, 58–64. doi:10.1016/j.commatsci.2019.05.039

Zhang, C., Liu, C., and Li, Q. (2019). Multi-factor evaluation method for the assessment of trans-critical organic Rankine cycle with low GWP fluids. *Energy Procedia* 158, 1626–1631. doi:10.1016/j.egypro.2019.01.380

Zhang, L., Liu, C., Li, Q., Wang, S., Cai, S., and Huo, E. (2022). Shale gas transport through the inorganic cylindrical and conical nanopores: a density gradient driven molecular dynamics. *Int. J. Heat Mass Transf.* 183, 122126. doi:10.1016/j.ijheatmasstransfer.2021.122126

Zheng, J., Barpaga, D., Trump, B. A., Shetty, M., Fan, Y., Bhattacharya, P., et al. (2020). Molecular insight into fluorocarbon adsorption in pore expanded metal–organic framework analogs. *J. Am. Chem. Soc.* 142 (6), 3002–3012. doi:10.1021/jacs.9b11963

Zhou, Y., Li, Q., and Wang, Q. (2019). Energy storage analysis of UIO-66 and water mixed nanofluids: an experimental and theoretical study. *Energies* 12 (13), 2521. doi:10.3390/en12132521

Zhu, Y., Li, W., Wang, Y., Li, H., and Li, S. (2021). Thermodynamic analysis and parametric optimization of ejector heat pump integrated with organic Rankine cycle combined cooling, heating and power system using zeotropic mixtures. *Appl. Therm. Eng.* 194, 117097. doi:10.1016/j.applthermaleng.2021.117097